Applied Catalysis B: Environmental 91 (2009) 347–354

Contents lists available at ScienceDirect

Applied Catalysis B: Environmental

journal homepage: www.elsevier.com/locate/apcatb

The dependence of catalytic activity for N_2O decomposition on the exchange extent of cobalt or copper in Na-MOR, H-MOR and Na-MFI

Maria Cristina Campa [a,*], Valerio Indovina [b], Daniela Pietrogiacomi [b]

[a] Sezione "Materiali Inorganici e Catalisi Eterogenea" dell'Istituto ISC (CNR) c/o Dipartimento di Chimica, "Sapienza" Università di Roma, Piazzale Aldo Moro 5, 00185 Roma, Italy
[b] Dipartimento di Chimica, "Sapienza" Università di Roma, Piazzale Aldo Moro 5, 00185 Roma, Italy

ARTICLE INFO

Article history:
Received 22 April 2009
Received in revised form 27 May 2009
Accepted 30 May 2009
Available online 10 June 2009

Keywords:
N_2O decomposition
Co-MOR
Cu-MOR
Co-nitrosyls

ABSTRACT

Catalytic decomposition of N_2O was studied on Na-MOR, H-MOR, and Na-MFI samples exchanged to various extents with cobalt or copper. Co-MOR samples were characterized by FTIR and volumetric measurements of NO adsorption. The most abundant species on Co-MOR was $Co^{2+}(NO)_2$. In agreement, the volumetric data yielded NO/Co = 1.8 ± 0.2.

On Co-MOR, N_2O conversion progressively increased as the cobalt content increased. All samples yielded similar apparent activation energy, E_a = 75 ± 5 kJ mol^{-1}. The reaction order was 0.9 ± 0.1 for N_2O, and 0.0 ± 0.1 for O_2. For samples having a Co-exchange percentage up to 61%, the turnover frequency *per* total Co atom was independent of the cobalt content and was significantly lower for more extensively exchanged samples. On all Co-MOR samples, the turnover frequency *per* isolated Co atom was nearly constant, indicating isolated Co^{2+} as the active site.

On Cu-MOR and Cu-MFI samples, N_2O conversion markedly increased with the copper content. Samples having a Cu-exchange percentage up to 62% yielded higher E_a than more extensively exchanged samples (150 ± 5 kJ mol^{-1} vs. 100 ± 5 kJ mol^{-1}). The reaction order was 0.5 ± 0.1 for N_2O, and 0.0 ± 0.1 for O_2.

We conclude that in Co-MOR and Co-MFI catalysts the active site for N_2O decomposition is isolated Co^{2+}, whereas in Cu-MOR and Cu-MFI isolated Cu^{2+} is nearly inactive. In extensively exchanged Cu-MOR and Cu-MFI, the active site for N_2O decomposition is most probably Cu^{1+}. A similar reaction mechanism for N_2O decomposition operates over Co-zeolites and extensively exchanged Cu-zeolites.

1. Introduction

Cobalt and copper exchanged zeolites are of paramount importance for various environmental catalytic reactions, such as NO abatement with reducing agents, NO decomposition and N_2O decomposition. Specifically, cobalt-exchanged zeolites (MFI, MOR, FER, BEA) are active for the selective catalytic reduction of NO with methane in the presence of oxygen [1–13]. Cu-MFI has unusually high activity for the catalytic decomposition of NO [14–19].

The catalytic activity of zeolites for NO decomposition, N_2O decomposition, and the abatement of NO with methane in the presence of oxygen (SCR) depends on three features: the zeolite type, the transition metal ion, and the extent of transition metal ion exchange.

As catalysts for NO decomposition, MFI extensively exchanged or over-exchanged with copper are active, whereas MFI exchanged to a lower extent are nearly inactive [14–19].

As catalysts for N_2O decomposition, cobalt and copper extensively exchanged in MOR and MFI are highly active [20]. Conversely, when exchanged in Y zeolite, the same transition metal ions are nearly inactive [20]. Only extensively exchanged Cu-MFI are highly active for N_2O decomposition [19], whereas the catalytic activity of Co-MFI depends linearly on the cobalt content [13]. The dependence of catalytic activity on the copper content is less clear in Cu-MOR [19] and its dependence on the cobalt content has not been investigated in Co-MOR [13].

For the abatement of NO with methane in the presence of oxygen by selective catalytic reduction (SCR), in an earlier study we found that the catalytic activity of Co-MFI [7] and Co-MOR [12] is proportional to the cobalt content. Whereas some invoke isolated Co^{2+} as the active site for this SCR reaction [1,7,10–12,21–23], others have suggested a role for a multinuclear cobalt oxo-alike species, of unspecified chemical composition [24–30]. Experiments conducted by our group [31] have shown that in Co-MOR exchanged with cobalt to various extents isolated Co^{2+} is the most abundant species (increasing from 86% to 100% as the cobalt content decreases), the residual cobalt being present as $[Co–O–Co]^{2+}$, and $[Co–O–Co]^{2+}$ alone is not the active site for NO abatement.

* Corresponding author. Fax: +39 06 490324.
E-mail address: mariacristina.campa@uniroma1.it (M.C. Campa).

0926-3373/$ – see front matter © 2009 Elsevier B.V. All rights reserved.
doi:10.1016/j.apcatb.2009.05.042

In this paper we studied the dependence of the catalytic activity for N_2O decomposition on the extent of transition metal ion exchange in Co-MOR, Co-MFI, Cu-MOR, and Cu-MFI. Our primary aim was to identify the active site for N_2O decomposition, define its nuclearity and oxidation state, and clarify the reaction mechanism. The Co-MFI samples used in this investigation resemble those we previously characterized by FTIR using CO and NO as probe molecules, and volumetric adsorption of CO and NO [7]. Analogously, the Co-MOR samples are nearly identical to or portions of those we previously characterized by FTIR using CO as a probe molecule and volumetric adsorption of CO [12,31]. In this investigation, we further characterized Co-MOR samples by FTIR using NO as a probe molecule, and volumetric adsorption of NO.

2. Experimental

2.1. Catalysts

Co-exchanged zeolites, Cu-exchanged zeolites and the starting materials for their preparation are listed in Table 1. Na-MOR (Si/Al = 9.2), H-MOR (Si/Al = 9.2), and Na-MFI (Si/Al = 11.9), kindly supplied by Tosoh Corporation, were used for ion exchange. In Na-MOR and in Na-MFI samples, the analytical Na content equalled the Al content calculated from the analytical Si/Al ratio given by the supplier. Cobalt or copper containing samples were ion exchanged at 350 K by contacting a weighted amount of zeolite (MOR or MFI) with an aqueous solution of cobalt acetate or copper acetate, as required. To obtain extensively exchanged samples, up to three exchange procedures were run in sequence. After the exchange procedure, samples were thoroughly washed with distilled water, dried overnight at 383 K, and calcined in air at 773 K for 5 h.

The sodium, the cobalt and the copper content of wet samples (equilibrated at ca. 79% relative humidity over a saturated solution of NH_4Cl) were determined by atomic absorption (Varian SpectrAA-30), and expressed as Na^+/Al, $2Co^{2+}$/Al or $2Cu^{2+}$/Al ratios. Exchanged samples are labeled as Me-X-ZEO-*a*-*b*, where Me specifies the transition metal ion exchanged (Co or Cu), X specifies the zeolite used in the preparation (H or Na), ZEO specifies the type of zeolite (MOR or MFI), *a* is the Si/Al ratio value, and *b* is the analytical metal ion exchange percentage, calculated assuming that *one* Me corresponded to *two* Al atoms (Table 1).

The Co_3O_4/Co-Na-MOR-9.2-92 sample was prepared by impregnating a portion of the Co-Na-MOR-9.2-92 sample with a solution of cobalt acetate. The sample was thereafter dried overnight at 383 K and calcined at 823 K for 5 h.

2.2. FTIR measurements

IR spectra on Co-Na-MOR-9.2 were run at RT on an FTIR spectrometer (Perkin-Elmer 2000) operated at a resolution of 4 cm^{-1}. The powdered samples were pelletted (pressure, 2×10^4 kg cm^{-2}) in self-supporting disks of ca. 10 mg cm^{-2}, and put in an IR cell which allowed thermal treatments in vacuum or in a controlled atmosphere. Before adsorption of NO (AIR LIQUIDE/SIO, 99.0%), catalysts were heated with O_2 (SOL, 99.9%) at 793 K for 1 h and evacuated at the same temperature for 1 h. For band integration and curve fitting we used the software program "Curvefit in Spectra Calc." (Galactic Industries).

2.3. Volumetric adsorption measurements

Volumetric adsorption experiments on Co-Na-MOR-9.2 were run at 298 K in a BET apparatus connected to an all-glass circulation system equipped with a magnetically driven pump, a pressure transducer (1.33×10^{-3} to 133.32 kPa, MKS Baratron) and a trap placed downstream from the reactor and kept at RT or 77 K, as specified. The catalyst (0.1 g) was placed in a temperature controlled silica adsorption chamber, thermoregulated at ±1.5 K. Before experiments, samples were heated in dry oxygen (about 8.00 kPa, trap at 77 K) at 773 K for 30 min and thereafter evacuated at the same temperature for 60 min. Adsorption of NO was measured according to the double isotherm method (pressure from 6.67×10^{-1} to 10.67 kPa), as proposed by Weller [32]. After determination of the first isotherm, the sample was evacuated for 30 min at the adsorption temperature, and a second isotherm was measured. The amount of NO adsorbed is given as STP volume per gram of catalyst (cm^3 g^{-1}), or as adsorbed molecules per total Co atoms (NO/Co). The amount of gas adsorbed during the first isotherm and that in the second isotherm, both determined by extrapolation at $p = 0$, will be referred as (i) total and (ii) reversible adsorption, respectively, and the difference (i)–(ii), as "irreversible" adsorption.

Table 1
Cobalt- or copper-exchanged zeolites (MOR or MFI): starting materials for sample preparation, analytical cobalt, copper and sodium amounts.

Starting materials	Catalysts	Na^+/Al	$2Me^{2+}$/Al[a]
Na-MOR-9.2		1.05	
	Cu-Na-MOR-9.2-20	0.82	0.20
	Cu-Na-MOR-9.2-39	0.67	0.39
	Cu-Na-MOR-9.2-47	0.57	0.47
	Cu-Na-MOR-9.2-100	0.36	1.05
	Co-Na-MOR-9.2-6	0.93	0.06
	Co-Na-MOR-9.2-11	0.91	0.11
	Co-Na-MOR-9.2-23	0.79	0.23
	Co-Na-MOR-9.2-41	0.57	0.41
	Co-Na-MOR-9.2-61	0.40	0.61
	Co-Na-MOR-9.2-92	0.36	0.92
	Co-Na-MOR-9.2-104	0.28	1.04
Co-Na-MOR-9.2-92	Co_3O_4/Co-Na-MOR-9.2-92	0.36	1.26
H-MOR-9.2			
	Co-H-MOR-9.2-24		0,24
Na-MFI-11.9		1.00	
	Cu-Na-MFI-11.9-22		0.22
	Cu-Na-MFI-11.9-42		0.42
	Cu-Na-MFI-11.9-62		0.62
	Cu-Na-MFI-11.9-93	0.17	0.93
	Cu-Na-MFI-11.9-125	0.05	1.25
	Co-Na-MFI-11.9-15	0.79	0.15
	Co-Na-MFI-11.9-39	0.70	0.39
	Co-Na-MFI-11.9-92	0.05	0.92

[a] Me^{2+}/Al is Cu^{2+}/Al or Co^{2+}/Al, depending on the catalyst.

2.4. Catalytic experiments

The catalytic activity was measured in a flow apparatus at atmospheric pressure. The apparatus included a feeding section where three gas streams (He, 3% N_2O in He, 15% O_2 in He) were regulated by means of independent mass flow controller-meters (MKS mod. 1259, driven by a four-channel unit MKS mod. 247 c) and mixed in a glass ampoule before entering the reactor. Gas mixtures were purchased from RIVOIRA and used without further purification. The reactor was made of silica with an internal sintered frit of about 12 mm diameter supporting the powdered catalyst (0.1 g). In all experiments, reactants and products were analyzed by gas chromatography. The gas chromatograph (Varian Micro-GC CP-4900) was equipped with two columns: (i) 10 m Molsieve 5A BF, for detecting N_2, and O_2, and (ii) 10 m Poraplot Q, for detecting N_2O.

A fresh portion of catalyst was treated in a flow of 2.5% O_2/He mixture (100 cm^3 min^{-1}), while the reactor was heated from room temperature to 773 K in about 45 min and then isothermally at 773 K for 90 min. After this treatment, the reactor was bypassed and the temperature adjusted to the desired value. Catalysis was

generally run with 4000 ppm (v/v) of N_2O in He. The reaction temperature was changed at random without intermediate activation treatment. The total flow rate was maintained at 50 cm^3 STP/min, and space velocity (GHSV) was 15 000 h^{-1}, based on the apparent sample density of 0.5 g cm^{-3}. To test catalyst stability, in some cases experiments lasted up to 25 h.

Percent N_2O conversion and N_2O decomposition rate (R_{N_2O}/molecules s^{-1} g^{-1}) were calculated from N_2O molecules consumed. In all experiments, we controlled that the amount of consumed N_2O equalled that of produced N_2 and was twice that of produced O_2. For each catalyst, apparent activation energy values (E_a/kJ mol^{-1}) were calculated from experiments in which the N_2O conversion did not exceed 20% ($\log R_{N_2O}$ vs. $1/T$). Turnover frequencies (N/molecules s^{-1} $atom^{-1}$) have been calculated as $N = R_{N_2O}/[L]$, where R_{N_2O} is the specific velocity (R_{N_2O}/molecules s^{-1} g^{-1}) and [L] is the concentration of active sites ([L]/atoms g^{-1}).

The reaction order in N_2O was determined by changing the N_2O content from 600 to 12 000 ppm in He. The dependence of R_{N_2O} on the O_2 content was determined by changing the O_2 content from 6000 to 45 000 ppm in He, maintaining the N_2O content constant at 4000 ppm.

3. Results and discussion

3.1. Sample characterization

Co-MOR samples were nearly identical to or portions of those used in previous investigations from our laboratory, whose FTIR characterization with CO has been detailed elsewhere [12,31]. In this investigation, Co-MOR samples were further characterized with FTIR using NO as a probe molecule and volumetric adsorption of NO.

3.1.1. FTIR of adsorbed carbon monoxide

Cobalt species present in Co-Na-MOR-9.2 samples, either heated in O_2 at 793 K and evacuated at the same temperature, or heated in O_2 at 793 K for 1 h, evacuated at the same temperature, and reduced with CO at increasing temperature up to 623 K, were identified by FTIR using CO adsorption at 298 K [12,31].

Co-Na-MOR-9.2 samples contained three types of cobalt species: isolated Co^{2+} in the main channels (α sites), isolated Co^{2+} in the smaller channels (β sites), and $[Co–O–Co]^{2+}$ species. The relative amount of the three species depended on the cobalt content. In particular, isolated Co^{2+} was the most abundant species present in all Co-Na-MOR-9.2 samples, decreasing from 100% to 86% as the cobalt content increased. Irrespective of the cobalt content, the ratio (Co^{2+} in α sites)/(Co^{2+} in β sites) was constant in all Co-Na-MOR-9.2.

After exposure of samples to CO at RT, FTIR showed that only a minute fraction of $[Co–O–Co]^{2+}$ underwent reduction yielding $[(CO)_nCo^+$-□-$Co^+(CO)_n]$, with n = 2 or 3, and CO_2. After exposure to CO at increasing temperature up to 623 K, the subsequent adsorption of CO at RT yielded increasing amount of $[(CO)_nCo^+$-□-$Co^+(CO)_n]$, and CO_2. Whereas isolated Co^{2+} did not undergo reduction, Co^{2+} in $[Co–O–Co]^{2+}$ reduced to Co^+. On evacuation at RT, $[(CO)_3Co^+$-□-$Co^+(CO)_3]$ completely and reversibly transformed into $[(CO)_2Co^+$-□-$Co^+(CO)_2]$. On evacuation at increasing temperature, $[(CO)_2Co^+$-□-$Co^+(CO)_2]$ progressively disappeared and transformed into a stable bridged species, $[Co^+(CO)Co^+]$, and $[(CO)Co^+$-□-$Co^+(CO)]$.

The $[Co–O–Co]^{2+}$ amount, determined from the integrated intensity of $Co^+(CO)_2$ bands, exponentially increased with the cobalt content. In the sample Co-Na-MOR-9.2-92, the percentage of Co^{2+} yielding the $[Co–O–Co]^{2+}$ species reached its maximum value, 14% of the total cobalt [31].

3.1.2. FTIR of adsorbed nitric oxide

In the spectral region 2300 to 1550 cm^{-1}, the adsorption of NO at RT on H-MOR-9.2, and Na-MOR-9.2 yielded extremely weak bands, whose intensity increased only slightly with increasing NO pressure, from 1.33×10^{-3} to 13.33 kPa (spectra not shown). On evacuation at RT for 10 min, all these bands nearly disappeared. The H-MOR-9.2 spectra consisted of weak bands from (i) N_2O at 2247 with a shoulder at 2230 cm^{-1}, (ii) NO^+ or $NO_2^{\delta+}$ at 2160 cm^{-1}, and (iii) nitrosyls at 1966 with shoulders at 2000, 1920 and 1900 cm^{-1}. The Na–MOR-9.2 spectra consisted of extremely weak bands from (i) N_2O at 2263 with a shoulder at 2240 cm^{-1}, and (ii) Na^+-nitrosyls at 1890 cm^{-1}. All these bands have been observed and assigned in previous investigations on MFI [33–36].

On all Co-MOR-9.2, in addition to the very weak bands of the corresponding H-MOR-9.2 and Na-MOR-9.2 matrices, NO adsorption at RT yielded new bands in the region 2300–1700 cm^{-1}. To characterize these bands, we investigated their intensity dependence on NO pressure, intensity dependence on the Co-exchange extent, and stability under evacuation at increasing temperature.

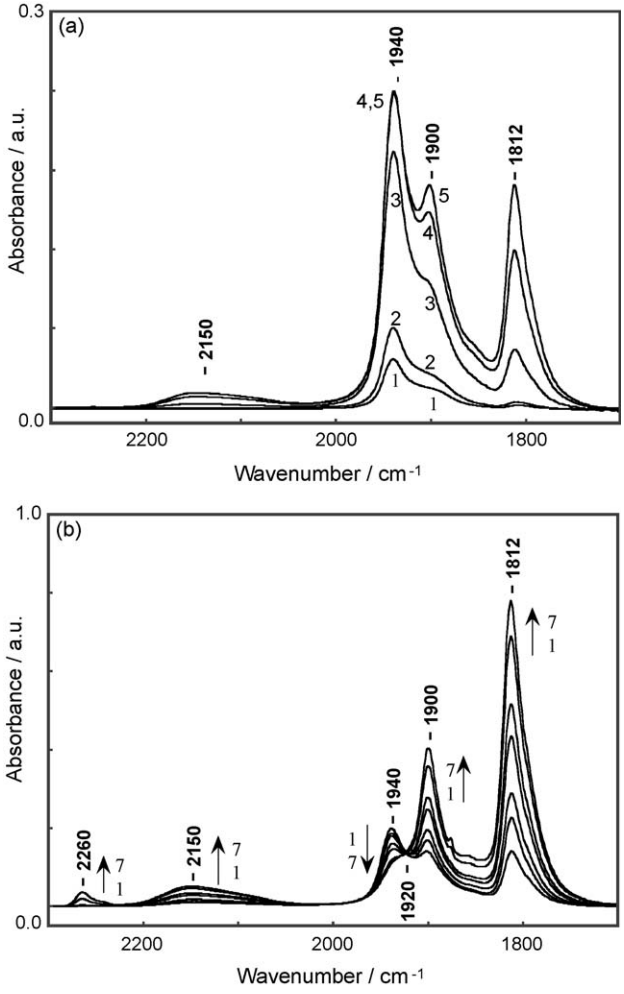

Fig. 1. FTIR spectra of NO adsorbed at RT on Co-Na-MOR-9.2-23. Section a. Addition of two small NO doses, corresponding to about NO/Co = 10^{-3} (first dose, spectrum 1; second dose, spectrum 2). In the subsequent NO additions, the equilibrium pressures were: $P_{NO} = 5.33 \times 10^{-3}$ kPa (spectrum 3); $P_{NO} = 8.00 \times 10^{-3}$ kPa (spectrum 4), $P_{NO} = 9.33 \times 10^{-3}$ kPa (spectrum 5). Section b. Equilibrium pressures: $P_{NO} = 9.33 \times 10^{-3}$ kPa (spectrum 1, as spectrum 5 in section a), 9.33×10^{-3} kPa, after 20 min of contact (spectrum 2), 8.00×10^{-2} kPa (spectrum 3), 4.00×10^{-1} kPa (spectrum 4), 1.07 kPa (spectrum 5), 6.40 kPa (spectrum 6), 10.67 kPa (spectrum 7).

FTIR experiments designed to study the extent to which the bands in the 2300–1700 cm^{-1} region depend on NO pressure showed that on all Co-MOR-9.2 samples, when a minute NO dose, about NO/Co $\cong 10^{-3}$, was added to the sample, a complex absorption band appeared with components at 1940 and 1900 cm^{-1} (Fig. 1a, spectrum 1). When two further NO doses were added in sequence, the intensity of all bands increased, particularly that of the band at 1940 cm^{-1}. New absorptions appeared at 1860 (shoulder) and 1812 cm^{-1}, the 1812 cm^{-1} absorption band being asymmetric in the low-frequency region (Fig. 1a, spectra 2 and 3). When further NO doses were added, the intensity of all bands increased further, the band at 1900 cm^{-1} also sharpened and a broad absorption band appeared at 2150 cm^{-1} (Fig. 1a, spectra 4 and 5). As the equilibrium pressure was increased from 9.33×10^{-3} to 10.67 kPa, the intensity of the 1940 cm^{-1} band progressively decreased, whereas all the other bands increased in intensity and a new weak band appeared at 2260 cm^{-1} (Fig. 1b, spectra 1–7). At about 1920 cm^{-1}, an isosbestic point was identified, indicating that the species absorbing at 1940 cm^{-1} had transformed into a species absorbing at 1900 cm^{-1}.

As the Co-exchange extent increased, all bands in the 2300–1700 cm^{-1} region increased (Fig. 2a and b). On Co-MOR-9.2 samples with Co-exchange extent $\geq$41, the admission of NO yielded new bands at about 1965 and 1985 cm^{-1} detected as shoulders on the aforementioned complex absorption at 1940 cm^{-1}. These bands also markedly increased in intensity with Co content (Fig. 2a and b).

The stability of bands in the 2300–1700 cm^{-1} region was investigated on Co-Na-MOR-9.2-92 by evacuation at increasing temperature from RT to 633 K. When this sample was evacuated at RT for 30 min, all bands decreased slightly in intensity (Fig. 3a, spectrum 1). On evacuation at increasing temperature from RT to 430 K, the intensity of bands at 2160, 1900 and 1812 cm^{-1} markedly decreased, whereas that of the band at 1940 cm^{-1} was partially restored (Fig. 3a, spectra 2 and 3). On evacuation at 503 K, the band at 2160 cm^{-1} disappeared and all the other bands decreased (Fig. 3a, spectrum 4). At 548 K, a new band at 1858 cm^{-1} appeared and that at 1940 cm^{-1} shifted to 1957 cm^{-1} (Fig. 3b, spectrum 1). At higher temperature, the band at 1957 cm^{-1} disappeared, those at 1900 and

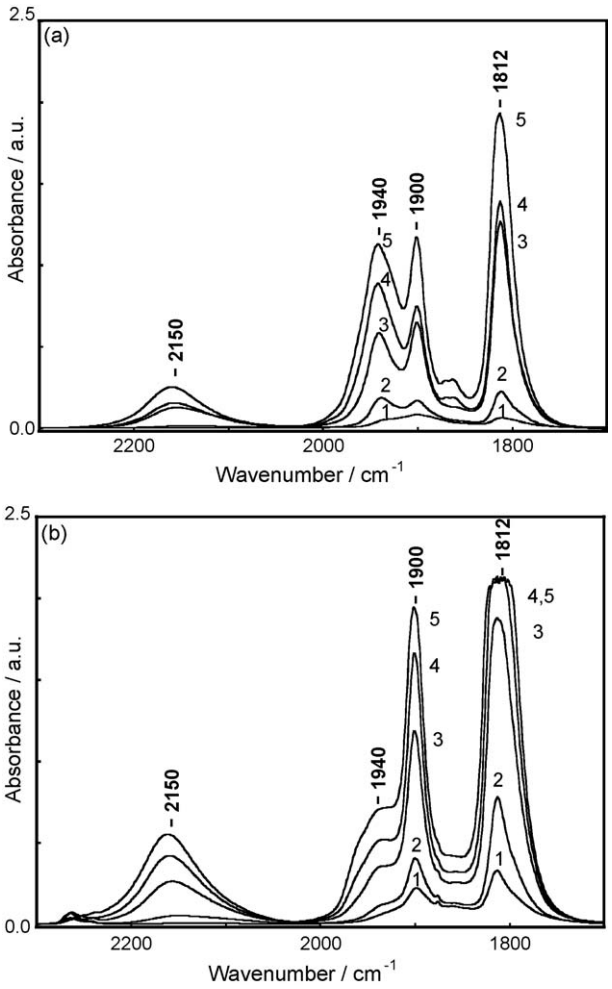

Fig. 2. FTIR spectra of NO adsorbed at RT on Co-Na-MOR-9.2 samples. Spectra recorded in the presence of NO at two equilibrium pressures: $P_{NO} = 9.33 \times 10^{-3}$ kPa (Section a); $P_{NO} = 12.00$ kPa (Section b). Catalysts: Co-Na-MOR-9.2-10 (spectrum 1); Co-Na-MOR-9.2-23 (spectrum 2); Co-Na-MOR-9.2-41 (spectrum 3); Co-Na-MOR-9.2-61 (spectrum 4); Co-Na-MOR-9.2-92 (spectrum 5).

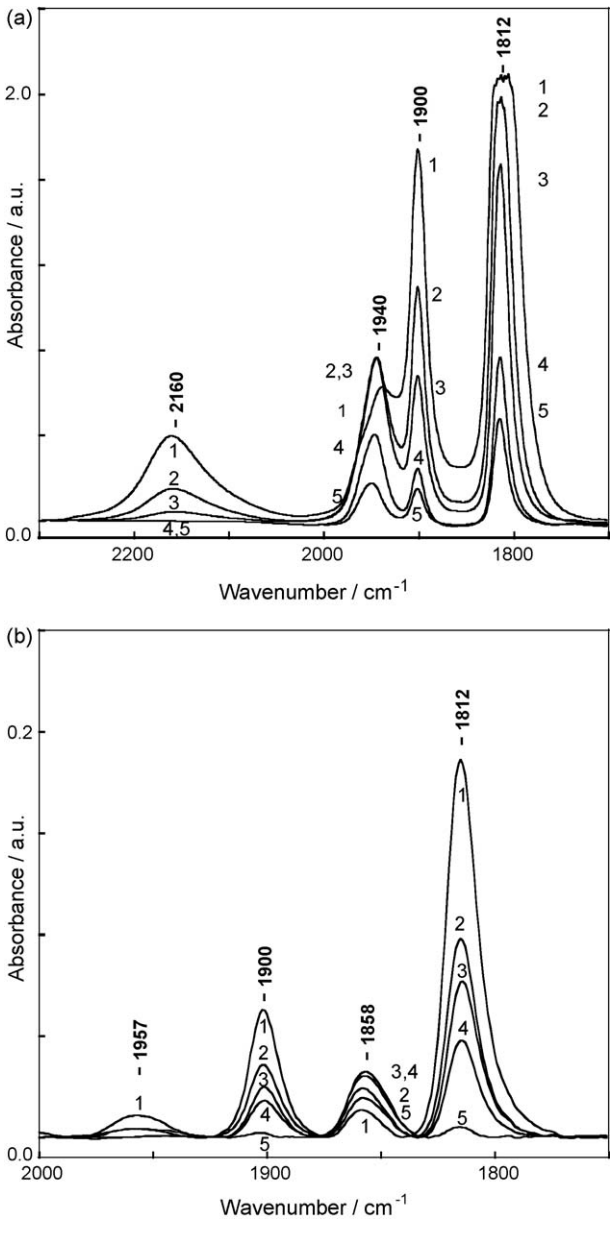

Fig. 3. FTIR spectra of NO adsorbed at RT on Co-Na-MOR-9.2-92 sample, after evacuating shortly at increasing temperature. Section a. Evacuation at $T = 298$ K (spectrum 1); $T = 373$ K (spectrum 2); $T = 430$ K (spectrum 3); $T = 503$ K (spectrum 4); $T = 523$ K (spectrum 5). Section b. Evacuation at $T = 548$ K (spectrum 1); $T = 558$ K (spectrum 2); $T = 573$ K (spectrum 3); $T = 598$ K (spectrum 4); $T = 633$ K (spectrum 5).

1812 cm^{-1} decreased, and that at 1858 cm^{-1} increased slightly (Fig. 3b, spectra 2–4). At 633 K, the 1858 cm^{-1} band was nearly the only one present (Fig. 3b, spectrum 5).

Bands in the 2000–1700 cm^{-1} region have been previously observed on various Co-zeolites [7,37–45], and assigned to mononitrosyls and dinitrosyls of cobalt. By consensus [7,37–45], the band at about 1900 cm^{-1} is the symmetric stretching mode of $Co^{2+}(NO)_2$ and that at 1812 cm^{-1} the asymmetric stretching mode of this dinitrosyl. The asymmetry and broadness of these two bands strongly suggest the concomitant presence of various $Co^{2+}(NO)_2$. The complex absorption centred at about 1940 cm^{-1} is typical of Co-mononitrosyls, whose cobalt oxidation state remains debatable [7,37–45]. Two observations suggest that the complex band at 1940 cm^{-1} contains an intense component arising from Co^{2+}–NO. First, as the NO equilibrium pressure increases, the intensity of the band at 1940 cm^{-1} decreases and the intensity of the two bands from $Co^{2+}(NO)_2$ increases concomitantly (isosbestic point at about 1920 cm^{-1}, Fig. 1b, spectra 1–7). Second, when NO is evacuated at increasing temperature up to 430 K, the two bands from $Co^{2+}(NO)_2$ reversibly transform into the band at 1940 cm^{-1} (Fig. 3a, spectra 1–3). These observations notwithstanding, the broad, complex band we observed at 1940 cm^{-1} might also mask a Co^{3+}–NO component. Several authors have suggested that the band at 1940 cm^{-1} arises from Co^{3+}–NO [38–42,44,45]. As Hadjiivanov et al. [41] have clarified, when geminal species lose one of their ligands, the produced linear compounds are expected to adsorb between the symmetric and antisymmetric modes of the geminal complexes. In agreement, we assign the band at 1858 cm^{-1} to Co^{2+}–NO linear species, which formed upon evacuation at increasing temperature: evacuation caused $Co^{2+}(NO)_2$ to decompose, yielding Co^{2+}–NO. Collectively, the FTIR of adsorbed NO shows that various $Co^{2+}(NO)_2$ formed, at least one Co^{3+}-NO, and at least two Co^{2+}–NO. This high heterogeneity in the cobalt nitrosyl species is consistent with the broad FTIR bands we observed after NO adsorption.

3.1.3. Volumetric adsorption of NO

Both the *total* and *irreversible* NO adsorption markedly increased with Co content (Table 2, columns 2 and 3). The percentage of irreversibly adsorbed NO was relatively large and changed little with Co content. The NO/Co ratio, evaluated from total adsorption, was nearly independent of the Co amount in the sample, yielding NO/Co = 1.8 ± 0.2 (Table 2, column 4). The NO/Co value indicates that a large fraction of cobalt adsorbed two NO molecules, yielding $Co^{2+}(NO)_2$. Our finding that the NO/Co ratio is independent of the Co content agrees with the fact that the intensity of Co-nitrosyl IR bands increased proportionally to the Co content.

3.2. Catalytic activity

3.2.1. The activity of Co-exchanged zeolites

In the whole temperature range investigated (523–793 K), all Co-exchanged zeolites were active and stable as a function of the time on stream: throughout experiments lasting up to about 25 h conversion never decreased. Co-MOR-9.2 catalysts invariably yielded higher N_2O conversion than H-MOR-9.2 and Na-MOR-9.2, which was completely inactive up to 793 K (Fig. 4a). On Co-MOR-9.2 samples, as the Co-exchange extent increased, N_2O conversion increased in parallel up to a Co-exchange percentage of ≤61%, and levelled off when the Co-exchange extent increased further. Co-Na-MOR-9.2-23 and Co–H-MOR-9.2-24 containing cobalt in similar amounts (0.95×10^{20} and 0.94×10^{20} Co^{2+} atoms g^{-1}, respectively), but having markedly different Brønsted acid site amounts (0.60×10^{20} and 6.88×10^{20} H^+ atoms g^{-1}, respectively), yielded similar N_2O conversion, showing that Brønsted acid sites contributed nothing or almost nothing to catalytic activity (Fig. 4a). Brønsted acid sites in Co-Na-MOR-9.2 arose from $Co^{2+}(H_2O)_n$ introduced in Na-MOR-9.2 during the exchange process. $Co^{2+}(H_2O)_n$ underwent hydrolysis in the subsequent heating at 773 K, thereby causing Brønsted acid sites to form, as discussed in the details in refs. [12,31]. Co-Na-MOR-9.2-92 and Co_3O_4/Co-Na-MOR-9.2-92 yielded almost identical N_2O conversion, showing that supported Co_3O_4 neither contributed to nor inhibited the catalytic activity of the exchanged cobalt (Fig. 4a). On all Co-MOR-9.2 samples, the apparent activation energies for N_2O decomposition, calculated from $\log R_{N_2O}$ vs. 1/T (data not shown), were similar, being $E_a = 75 \pm 5$ kJ mol^{-1}. On all these samples, the reaction order in N_2O was 0.9 ± 0.1, and the reaction rate was independent of the O_2 content in the mixture.

The almost identical E_a and reaction orders on all Co-MOR-9.2 suggest further that a similar reaction mechanism operated over

Table 2
Adsorption of NO at RT on Co-MOR catalysts.

Catalysts	V_{STP}(NO)/cm^3 g^{-1}		NO/Co[a]
	Total	Irreversible	
H-MOR-9.2	0.9	0.9	
Co-H-MOR-9.2-24	6.9	6.8	1.7
Na-MOR-9.2	0.0	0.0	
Co-Na-MOR-9.2-11	2.7	2.1	1.7
Co-Na-MOR-9.2-23	6.5	5.6	1.8
Co-Na-MOR-9.2-41	12.5	11.3	2.0
Co-Na-MOR-9.2-92	21.5	18.0	1.6

[a] Calculated from total adsorption.

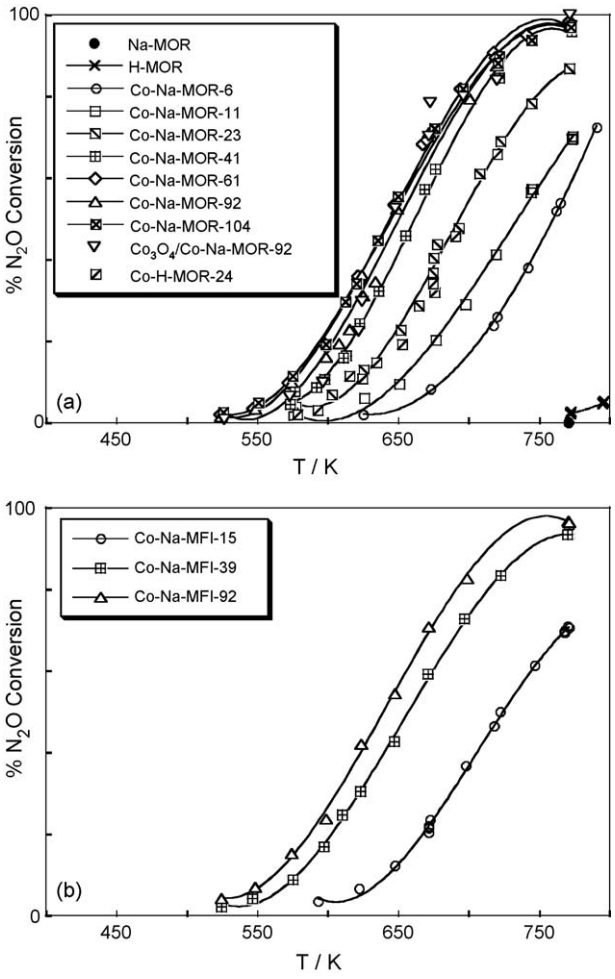

Fig. 4. Percent N_2O conversion as a function of temperature on Co-MOR-9.2 (Section a) and Co-MFI-11.9 (Section b).

all Co-MOR-9.2 samples, and involved the same active molecular complex. Under these conditions, namely a constant entropy factor and a constant activation energy, the only parameter which affects R_{N_2O} in passing from one sample to another is the concentration of active sites containing cobalt. The simplest assumption our data suggest for active sites is that all Co^{2+} ions were active. The concentration of active sites, [L]/sites g^{-1}, might be smaller than the total Co^{2+} concentration value, $[Co^{2+}]_{tot}$/atoms g^{-1}, for two reasons: a configurational factor, arising if the reaction requires an active site including only isolated ions, or, conversely, special clusters, such as $[Co–O–Co]^{2+}$, and a heterogeneity factor, arising from activity differences among cobalt species located in various sites within the zeolite matrix, such as Co^{2+} in the main channels or in the smaller channels. Assuming that all Co^{2+} ions were active, that is $[L] = [Co^{2+}]_{tot}$, we can calculate the turnover frequency as $N_{Co\ tot} = R_{N_2O}/[Co^{2+}]_{tot}$.

When we assumed that all Co^{2+} ions were equally active, and compared the various Co-MOR-9.2 catalysts in an Arrhenius plot reporting log $N_{Co\ tot}$ as a function of 1/T, we found that for samples with Co-exchange percentage up to 61%, $N_{Co\ tot}$ was independent of the total cobalt content (Fig. 5). For more extensively exchanged samples, $N_{Co\ tot}$ was significantly lower. On these samples, the $[Co–O–Co]^{2+}$ amount exponentially increased with the cobalt content, suggesting that $[Co–O–Co]^{2+}$ were inactive or much less active than isolated Co^{2+}. When we assumed that only isolated Co^{2+} ions were active, and calculated the turnover frequency as $N_{Co\ is} = R_{N_2O}/[Co^{2+}]_{is} = R_{N_2O}/([Co^{2+}]_{tot} - [Co–O–Co]^{2+})$ we found that $N_{Co\ is}$ was independent of the cobalt content, suggesting that all isolated Co^{2+} ions or a constant fraction of them were equally active (Fig. 6).

On Co-Na-MFI-11.9, the E_a values, the reaction order in N_2O and the reaction order in O_2 were nearly identical to the corresponding values on Co-Na-MOR-9.2. Although we studied the dependence of catalytic activity on the cobalt content in lesser detail for Co-Na-MFI-11.9 than for Co-Na-MOR-9.2 samples, the comparison between the two shows that the turnover frequency *per* total cobalt ion on Co-Na-MFI-11.9 was nearly equal to that on Co-Na-MOR-9.2, or somewhat higher (Fig. 7).

3.2.2. The activity of Cu-exchanged zeolites

On Cu-Na-MOR-9.2 and Cu-Na-MFI-11.9, N_2O conversion markedly increased with the copper content (Fig. 8a and b). The E_a values were 150 ± 5 kJ mol^{-1} on samples with Cu-exchange extent from 20% to 50%, and were lower on more extensively exchanged Cu-Na-MOR-9.2 and Cu-Na-MFI-11.9 samples, resulting $E_a = 100 \pm 5$ kJ mol^{-1}, suggesting that the active sites for N_2O conversion differed in the two exchange extent regions. On all samples, the reaction order in N_2O was 0.5 ± 0.1, and the reaction rate

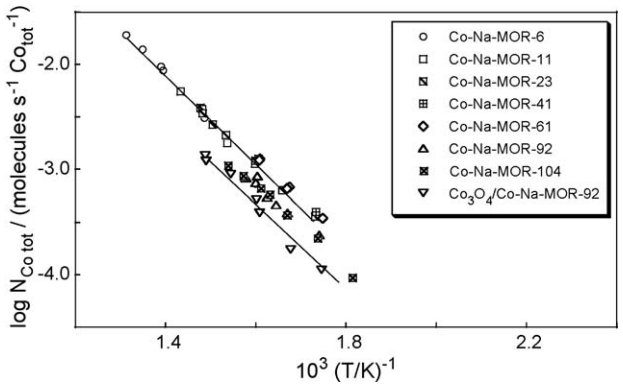

Fig. 5. Turnover frequency *per* total cobalt ion ($N_{Co\ tot}$/molecules s^{-1} Co_{tot}^{-1}) on Co-Na-MOR-9.2.

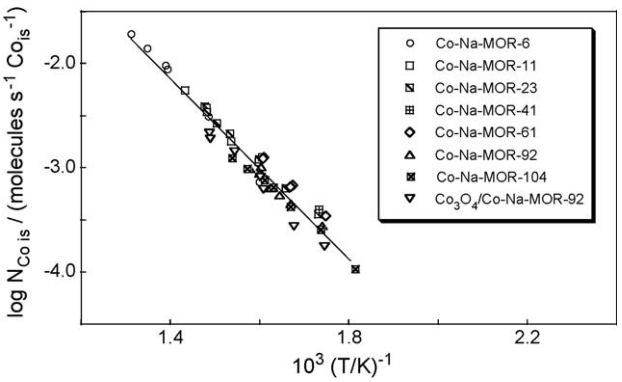

Fig. 6. Turnover frequency *per* isolated cobalt ion ($N_{Co\ is}$/molecules s^{-1} Co_{is}^{-1}) on Co-Na-MOR-9.2.

was independent of the O_2 content in the mixture. On both Cu-Na-MOR-9.2 and Cu-Na-MFI-11.9, R_{N_2O} (molecules s^{-1} g^{-1}) was very low on samples with Cu-exchange percentage up to 50%, and steeply increased on more extensively exchanged copper samples (Fig. 9a and b). This reaction rate dependence resembles that observed by Smeets et al. on Cu-MFI [19]. Our results extend Smeets et al's findings showing an analogous reaction rate dependence also on Cu-Na-MOR-9.2. At all copper contents, Cu-Na-MFI-11.9 samples were more active than Cu-Na-MOR-9.2.

3.2.3. The mechanism of N_2O decomposition and the oxidation state of the active site

The constant $N_{Co\ is}$ on Co-MOR-9.2 samples strongly suggests that all isolated cobalt ions or a constant fraction of them are active for the decomposition of N_2O. Active sites for N_2O decomposition must be endowed with high electron donor properties [46]. Ample evidence documenting the high electron donor properties of isolated Co^{2+} in MFI comes from O_2 adsorption, showing the formation of $Co^{3+}\cdots O^{2-}$adducts, as identified by electron spin resonance spectroscopy [47]. Others have already described analogous redox properties with O_2 and N_2O for cobalt in other matrices [48–51]. We therefore propose that the mechanisms operating for N_2O decomposition over Co-MOR-9.2 and Co-MFI-11.9 closely resembles that previously proposed by Kapteijn et al. [52], and recently by Smeets et al. for Co-MFI [13]. Specifically,

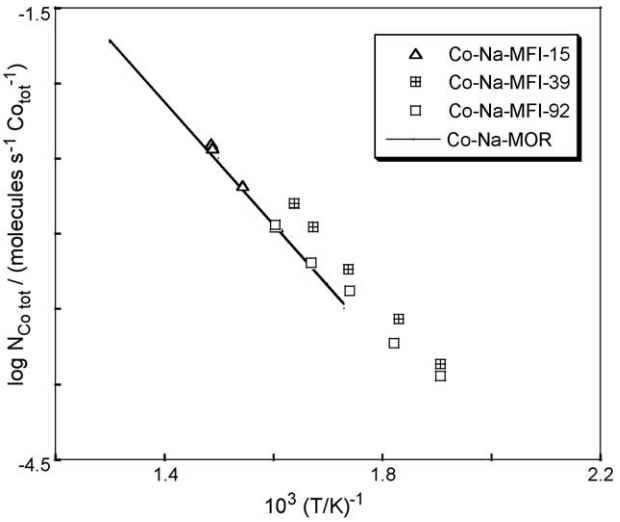

Fig. 7. Turnover frequency *per* total cobalt ion ($N_{Co\ tot}$/molecules s^{-1} Co_{tot}^{-1}) on Co-Na-MFI-11.9. A comparison with Co-Na-MOR-9.2.

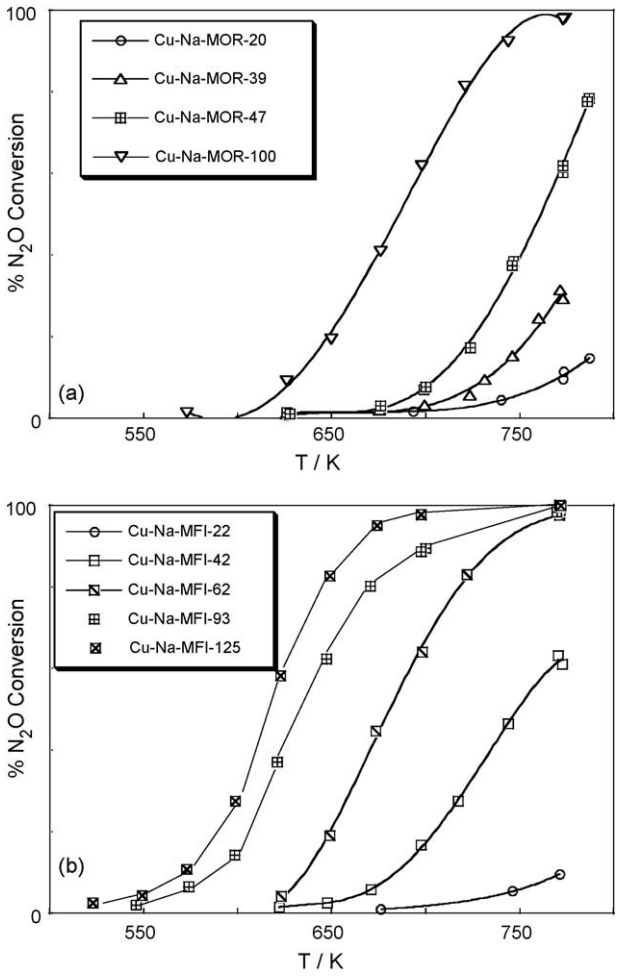

Fig. 8. Percent N_2O conversion as a function of temperature on Cu-Na-MOR-9.2 (Section a) and Cu-Na-MFI-11.9 (Section b).

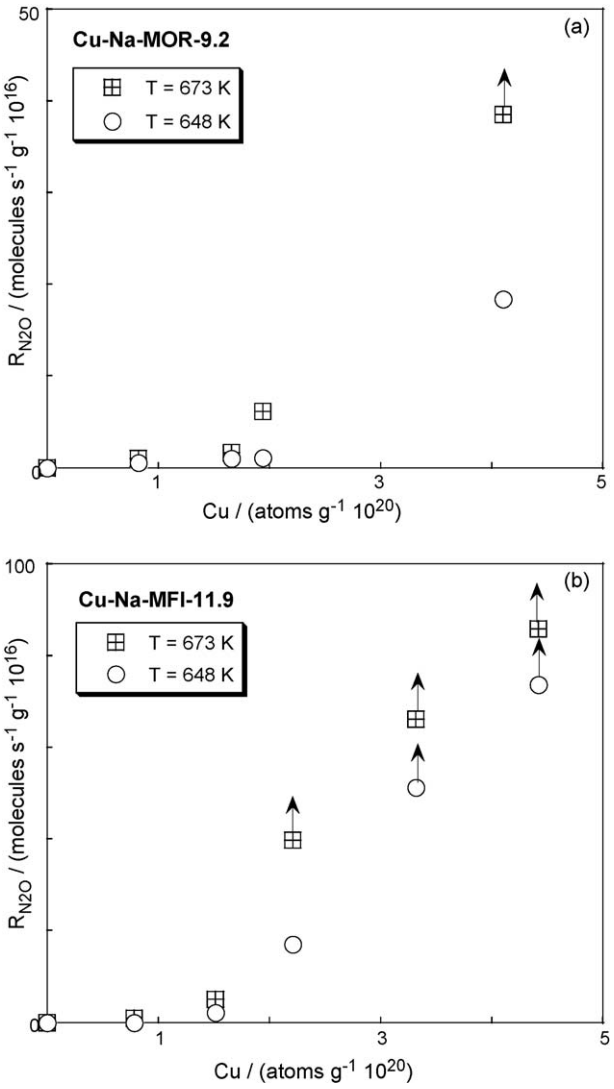

Fig. 9. Rates of N_2O decomposition at 648 K and 673 K (R_{N_2O}/ molecules s^{-1} g^{-1} × 10^{16}) as a function of Cu content (Cu/atoms g^{-1} × 10^{20}) on Cu-Na-MOR-9.2 (Section a) and Cu-Na–MFI-11.9 (Section b). Points marked with an arrow are R_{N_2O} lower limit values, being calculated from experiments in which conversion exceeds 20%.

isolated Co^{2+} decomposes N_2O, according to the following elementary steps:

$$Co^{2+} + N_2O_{(g)} \rightarrow Co^{3+}\cdots O^- + N_{2(g)}$$

$$Co^{3+}\cdots O^- + N_2O_{(g)} \rightarrow Co^{2+} + O_{2(g)} + N_{2(g)}$$

Conversely, the $[Co–O–Co]^{2+}$ species, present in the extensively exchanged Co-Na-MOR-9.2 samples, reacts with N_2O, stabilising oxygen in a strong oxidic form:

$$[Co–O–Co]^{2+} + N_2O_{(g)} \rightarrow [(O^{2-})\cdots Co^{3+}–O–Co^{3+}] + N_{2(g)}$$

The species $[(O^{2-})\cdots Co^{3+}–O–Co^{3+}]$ does not react with N_2O, thus making the $[Co–O–Co]^{2+}$ species inactive.

For Cu-exchanged zeolites, Smeets et al. [19] attributed the high activity of extensively exchanged Cu-MFI to the presence of bis(μ-oxo)dicopper species in these samples, and the low activity of low-extent exchanged Cu-MFI to their absence. Evidence for a role of this bis(μ-oxo)dicopper core, i.e. $[Cu_2(\mu\text{-}O)_2]^{2+}$, in the decomposition of N_2O on extensively exchanged Cu-MFI has been given by combining operando UV–vis spectroscopy and on-line GC analysis [53]. We propose a different explanation. Specifically, because Cu-Na-MFI-11.9 and Cu-Na-MOR-9.2 samples exchanged with copper to a low extent contain isolated Cu^{2+} ions alone, and these copper species do not possess electron donor properties, low-extent exchanged samples are therefore inactive for N_2O decomposition. Conversely, because extensively exchanged Cu-Na-MFI-11.9 and Cu-Na-MOR-9.2 contain Cu^{1+} species which are highly effective electron donor sites, these samples are therefore highly active for N_2O decomposition. The presence of Cu^{1+} in extensively exchanged Cu-MFI has been documented by FTIR [54,55], DRIFT [56], and redox cycle experiments [57]. Most probably, Cu^{1+} species arise from the reduction of Cu^{2+} pairs present in extensively exchanged Cu-zeolites, as others have suggested [57,58]. From the foregoing observations, at variance with Smeets et al., who suggested that the mechanism operating on Cu-MFI [19] differs from that operating on Co-MFI [13], we suggest that the mechanism operating on extensively exchanged Cu-Na-MOR-9.2 and Cu-Na-MFI-11.9 is the same as that operating on all Co-Na-MOR-9.2 and Co-Na-MFI-11.9. Namely, on extensively exchanged Cu-Na-MOR-9.2 and Cu-Na-MFI-11.9, the following elementary steps take place:

$$Cu^{1+} + N_2O_{(g)} \rightarrow Cu^{2+}\cdots O^- + N_{2(g)}$$

$$Cu^{2+}\cdots O^- + N_2O_{(g)} \rightarrow Cu^{1+} + O_{2(g)} + N_{2(g)}$$

4. Conclusions

In agreement with our previous FTIR characterization of Co-MFI with NO [7], the analogous characterization of Co-MOR confirms

that also in these samples a large fraction of cobalt is present as isolated Co^{2+} with two coordinative vacancies. The fact that $Co^{2+}(NO)_2$ is the most abundant species agrees with the volumetric NO adsorption data (NO/Co = 1.8 ± 0.2).

The constant turnover frequency *per* isolated Co^{2+} demonstrates that this is the active site for N_2O decomposition. Isolated Cu^{2+} in Cu-MFI and Cu-MOR is nearly inactive for N_2O decomposition. Most probably, Cu^{1+} is the active site in extensively exchanged Cu-MOR and Cu-MFI. We suggest that the same reaction mechanism operates in all Co-zeolites, irrespective of the cobalt content, and in the extensively exchanged Cu-zeolites.

Acknowledgements

We gratefully thank Dr. Cristina Tortolini and Dr. Luca Farina for preparing some Cu-and Co-zeolite samples and analyzing their chemical content.

References

[1] Y. Li, J.N. Armor, Appl. Catal. B 2 (1993) 239–256.
[2] Y. Li, J.N. Armor, J. Catal. 150 (1994) 376–387.
[3] F. Witzel, G.A. Sill, W.K. Hall, J. Catal. 149 (1994) 229–237.
[4] R. Burch, S. Scirè, Appl. Catal. B 3 (1994) 295–318.
[5] D.B. Lukyanov, G. Sill, J.L. d'Itri, W.K. Hall, J. Catal. 153 (1995) 265–274.
[6] D.B. Lukyanov, E.A. Lombardo, G.A. Sill, J.L. d'Itri, W.K. Hall, J. Catal. 163 (1996) 447–456.
[7] M.C. Campa, S. De Rossi, G. Ferraris, V. Indovina, Appl. Catal. B 8 (1996) 315–331.
[8] L.J. Lobree, A.W. Aylor, A. Reimer, A.T. Bell, J. Catal. 169 (1997) 188–193.
[9] J.R. Regalbuto, T. Zheng, J.T. Miller, Catal. Today 54 (1999) 495–505.
[10] D. Kaucký, A. Vondrová, J. Dědeček, B. Wichterlová, J. Catal. 194 (2000) 318–329.
[11] X. Wang, H. Chen, W.M.H. Sachtler, Appl. Catal. B 29 (2001) 47–60.
[12] M.C. Campa, I. Luisetto, D. Pietrogiacomi, V. Indovina, Appl. Catal. B 46 (2003) 511–522.
[13] P.J. Smeets, Q. Meng, S. Corthals, H. Leeman, R.A. Schoonheydt, Appl. Catal. B 84 (2008) 505–513.
[14] M. Iwamoto, H. Furukawa, Y. Mine, F. Uemura, S. Mikuriya, S. Kagawa, J. Chem. Soc., Chem. Commun. (1986) 1272–1273.
[15] Y. Li, W.K. Hall, J. Catal. 129 (1991) 202–215.
[16] M. Shelef, Chem. Rev. 95 (1995) 209–225.
[17] M.C. Campa, V. Indovina, G. Minelli, G. Moretti, I. Pettiti, P. Porta, A. Riccio, Catal. Lett. 23 (1994) 141–149.
[18] G. Moretti, G. Ferraris, G. Fierro, M. Lo Jacono, S. Morpurgo, M. Faticanti, J. Catal. 232 (2005) 476–487.
[19] P.J. Smeets, M.H. Groothaert, R.M. van Teeffelen, H. Leeman, E.J.M. Hensen, R.A. Schoonheydt, J. Catal. 245 (2007) 358–368.
[20] Y. Li, J.N. Armor, Appl. Catal. B 1 (1992) L21–L29.
[21] B. Wichterlová, Top. Catal. 28 (2004) 131–140.
[22] J. Dědeček, D. Kaucký, B. Wichterlová, Top. Catal. 18 (2002) 283–290.
[23] A.W. Aylor, L.J. Lobree, J.A. Reimer, A.T. Bell, in: J.W. Hightower, W.N. Delgass, E. Iglesia, A.T. Bell (Eds.), Studies in Surface Science and Catalysis, vol. 101, Elsevier Science Publ., Amsterdam, The Netherlands, 1996, pp. 661–670.
[24] J.A.Z. Pieterse, R.W. van den Brink, S. Booneveld, F.A. de Bruijn, Appl. Catal. B 46 (2003) 239–250.
[25] E.M. Sadovskaya, A.P. Suknev, L.G. Pinaeva, V.B. Goncharov, B.S. Bal'zhinimaev, C. Chupin, J. Pérez-Ramírez, C. Mirodatos, J. Catal. 225 (2004) 179–189.
[26] E.M. Sadovskaya, A.P. Suknev, V.B. Goncharov, B.S. Bal'zhinimaev, C. Mirodatos, Kinet. Catal. 45 (2004) 436–445.
[27] T. Montanari, O. Marie, M. Daturi, G. Busca, Catal. Today 110 (2005) 339–344.
[28] C. Chupin, A.C. van Veen, M. Konduru, J. Després, C. Mirodatos, J. Catal. 241 (2006) 103–114.
[29] M. Mihaylov, K. Hadjiivanov, Chem. Commun. (2004) 2200–2201.
[30] T. Montanari, O. Marie, M. Daturi, G. Busca, Appl. Catal. B 71 (2007) 216–222.
[31] V. Indovina, M.C. Campa, D. Pietrogiacomi, J. Phys. Chem. C 112 (2008) 5093–5101.
[32] S.W. Weller, Acc. Chem. Res. 16 (1983) 101–106.
[33] E. Giamello, D. Murphy, G. Magnacca, C. Morterra, Y. Shioya, T. Nomura, M. Anpo, J. Catal. 136 (1992) 510–520.
[34] J. Valyon, W.K. Hall, J. Phys. Chem. 97 (1993) 1204–1212.
[35] T.E. Hoost, K.A. Laframboise, K. Otto, Catal. Lett. 33 (1995) 105–116.
[36] K. Hadjiivanov, J. Saussey, J.L. Freysz, J.C. Lavalley, Catal. Lett. 52 (1998) 103–108.
[37] Y. Li, T.L. Slager, J.N. Armor, J. Catal. 150 (1994) 388–399.
[38] K. Hadjiivanov, B. Tsyntsarski, T. Nikolova, Phys. Chem. Chem. Phys. 1 (1999) 4521–4528.
[39] F. Geobaldo, B. Onida, P. Rivolo, F. Di Renzo, F. Fajula, E. Garrone, Catal. Today 70 (2001) 107–119.
[40] E. Ivanova, K. Hadjiivanov, D. Klissurski, M. Bevilacqua, T. Armaroli, G. Busca, Micropor. Mesopor. Mater. 46 (2001) 299–309.
[41] K. Hadjiivanov, E. Ivanova, M. Daturi, J. Saussey, J.-C. Lavalley, Chem. Phys. Lett. 370 (2003) 712–718.
[42] A. Mihaylova, K. Hadjiivanov, S. Dzwigaj, M. Che, J. Phys. Chem. B 110 (2006) 19530–19536.
[43] L.B. Gutierrez, E.E. Miró, M.A. Ulla, Appl. Catal. A 321 (2007) 7–16.
[44] K. Góra-Marek, B. Gil, M. Śliwa, J. Datka, Appl. Catal. A 330 (2007) 33–42.
[45] K. Góra-Marek, B. Gil, J. Datka, Appl. Catal. A 353 (2009) 117–122.
[46] A. Cimino, F.S. Stone, Adv. Catal. 47 (2002) 141–306.
[47] El-M. El-Malki, D. Werst, P.E. Doan, W.M.H. Sachtler, J. Phys. Chem. B 104 (2000) 5924–5931.
[48] R.F. Howe, J.H. Lunsford, J. Am. Chem. Soc. 97 (1975) 5156–5159.
[49] V. Indovina, D. Cordischi, M. Occhiuzzi, A. Arieti, J. Chem. Soc. Faraday Trans. I 75 (1979) 2177–2187.
[50] D. Cordischi, V. Indovina, in: M. Che, G.C. Bond (Eds.), Adsorption and Catalysis on Oxide Surfaces, Elsevier Science Publ., Amsterdam, The Netherlands, 1985, pp. 209–220.
[51] E. Giamello, Z. Sojka, M. Che, A. Zecchina, J. Phys. Chem. 90 (1986) 6084–6091.
[52] F. Kapteijn, J. Rodriguez-Mirasol, J.A. Moulijn, Appl. Catal. B 9 (1996) 25–64.
[53] M.H. Groothaert, K. Lievens, H. Leeman, B.M. Weckhuysen, R. Schoonheydt, J. Catal. 220 (2003) 500–512.
[54] G. Turnes Palomino, P. Fisicaro, S. Bordiga, A. Zecchina, E. Giamello, C. Lamberti, J. Phys. Chem. B 104 (2000) 4064–4073.
[55] F.X. Llabrés i Xamena, P. Fisicaro, G. Berlier, A. Zecchina, G. Turnes Palomino, P. Prestipino, S. Bordiga, E. Giamello, C. Lamberti, J. Phys. Chem. B 107 (2003) 7036–7044.
[56] P.E. Fanning, M.A. Vannice, J. Catal. 207 (2002) 166–182.
[57] P. Ciambelli, P. Corbo, M. Gambino, V. Indovina, G. Moretti, M.C. Campa, in: A. Frennet, J.-M. Bastin (Eds.), Studies in Surface Science and Catalysis, vol. 96, Elsevier Science Publ., Amsterdam, The Netherlands, 1995, pp. 605–617.
[58] M. Lo Jacono, G. Fierro, R. Dragone, X. Feng, J. d'Itri, W.K. Hall, J. Phys. Chem. B 101 (1997) 1979–1984.